PAPER • OPEN ACCESS

Optical simulations and optimization of perovskite/CI(G)S tandem solar cells using the transfer matrix method

View the article online for updates and enhancements.

Journal of Physics: Energy

PAPER

Optical simulations and optimization of perovskite/CI(G)S tandem solar cells using the transfer matrix method

Aleksandra Bojar[1,2,*] , Daniel Micha[1,3], Maxime Giteau[3], Marco A Ruiz-Preciado[4], Ulrich W Paetzold[4], Marcel Simor[5], Veronique S Gevaerts[5], Romain Carron[6], Karim Medjoubi[1], Stéphane Collin[1,3] , Negar Naghavi[1,2], Jean-François Guillemoles[1,2] and Philip Schulz[1,2,*]

1. IPVF, Institut Photovoltaïque d'Ile-de-France, 18, Boulevard Thomas Gobert, 91120 Palaiseau, France
2. CNRS, UMR 9006, 18, Boulevard Thomas Gobert, 91120 Palaiseau, France
3. Centre for Nanoscience and Nanotechnology (C2N), CNRS, Université Paris-Saclay, 91120 Palaiseau, France
4. Institute of Microstructure Technology, Karlsruhe Institute of Technology, 76344 Eggenstein-Leopoldshafen, Germany; Light Technology Institute, Karlsruhe Institute of Technology, 76131 Karlsruhe, Germany
5. TNO Partner in Solliance, Department of Solar Technology and Applications, NL-5656 AE, Eindhoven, The Netherlands
6. Laboratory for Thin films and Photovoltaics, EMPA—Swiss Federal Laboratories for Materials Science and Technology, Dübendorf, Switzerland
* Authors to whom any correspondence should be addressed.

E-mail: Aleksandra.Bojar@cnrs.fr and Philip.Schulz@cnrs.fr

Abstract

In this work we employ the transfer matrix method for the analysis of optical materials properties to simulate and optimize monolithic tandem solar cell devices based on $CuIn_{1-x}Ga_xSe_2$, CI(G)S, and perovskite (PVK) absorbers. By finding models that fit well the experimental data of the CI(G)S solar cell, the semitransparent perovskite solar cell (PSC) and the PVK/CI(G)S monolithic tandem solar cell, we were able to perform a detailed optical loss analysis that allowed us to determine sources of parasitic absorption. We found better substitute materials for the transport layers to increase the power conversion efficiency and, in case of semitransparent PSCs, sub-bandgap transmittance. Our results set guidelines for the monolithic PVK/CI(G)S tandem solar cells development, predicting an achievable efficiency of 30%.

1. Introduction

Tandem solar cells are one of the most efficient ways to overcome the limits of power conversion efficiency (PCE) of single junction solar cells and reach PCEs higher than 30% [1]. By combining two photo-absorber materials with different bandgaps, these devices can more efficiently convert the solar spectrum into electricity mainly due to a reduction of thermalization losses [2, 3]. Halide perovskite (PVK) materials are promising candidates for the top sub-cell absorber due to their large tunable bandgap [4, 5] steep absorption edge [6] and potential to be implemented via cost-effective fabrication processes [7], among the others. For more information about these materials, we recommend the following reviews [8–10]. Perovskite solar cells (PSCs) have been successfully combined with silicon bottom sub-cells in tandem configurations, reaching the highest efficiencies ever demonstrated (apart from III–V materials) of 32.5% for two-terminal (2T) configuration [1]. Despite the promising future of this technology, the research community is also searching for alternatives, which can potentially go along with mainstream silicon-based photovoltaics to help propel the transition towards renewable sources of energy. One of them is the use of $CuIn_{1-x}Ga_xSe_2$ CI(G)S as bottom sub-cell. These material offers the advantages of a compositional tunable bandgap in the range 1.03–1.68 eV combined with a high absorption coefficient, allowing for an all thin-film tandem technology [11–13]. Indeed, a combination of an only 500 nm thick PVK and 2500 nm thick CI(G)S absorber layer in a monolithic 2T tandem configuration has been demonstrated reaching efficiencies as high as 24.2% [14]. Although the efficiencies still lag behind those of PVK/Si tandems, they have a theoretical potential to reach

values higher than 40% [2]. Achieving this goal will require a dedicated optimization of the device layout with respect to its electrical and optical properties.

While the PCE optimization is generally more sensitive to deviations from the optimal bandgap energies, 2T tandems offer many advantages over their four-terminal (4T) counterpart. First and foremost, the need for only one transparent electrode decreases the fabrication costs and complexity, due to the use of less material and fewer deposition steps, and minimizes losses due to parasitic absorption. Furthermore, 2T tandems allow for an easier integration with current photovoltaic systems and hence many optimization efforts are focused on this tandem architecture [15]. The ongoing challenge to make this technology a success lies in developing high performing top sub-cells with high transmittance of the non-absorbed part of the solar spectrum allowing for current matching between the two sub-cells. Optical optimization directly addresses this issue by allowing the adjustment of the layers' thicknesses and materials in the stack leading not only to current matching but also lower parasitic absorption, as already suggested by Kurtz *et al* [16]. Since the layers considered in this work are thin film, using a simple Beer–Lambert model to estimate absorption is not enough. Instead, the transfer matrix method is a significantly more accurate model that accounts for interference/resonance effects that are present in thin film stacks. The most efficient approach to this is starting with an idealized design of the structure provided by device modeling and simulation, that can serve as a starting point for experimental optimization.

In this study, we used the transfer matrix method to simulate the optical performance of PVK/CI(G)S 2T tandem solar cells. With the aid of a refractive index database built with experimental data and supplemented with values from literature we show a thorough optimization of the device stack by increasing absorption in the relevant layers and transmittance in the relevant wavelength range, thus enhancing current matching and decreasing parasitic absorption. Moreover, our theoretical results are directly compared to experimental data for validation of the model and feedback into the optical model and database. In the end, this approach leads to the prediction of an optimized layer stack for high device performance.

2. Methods

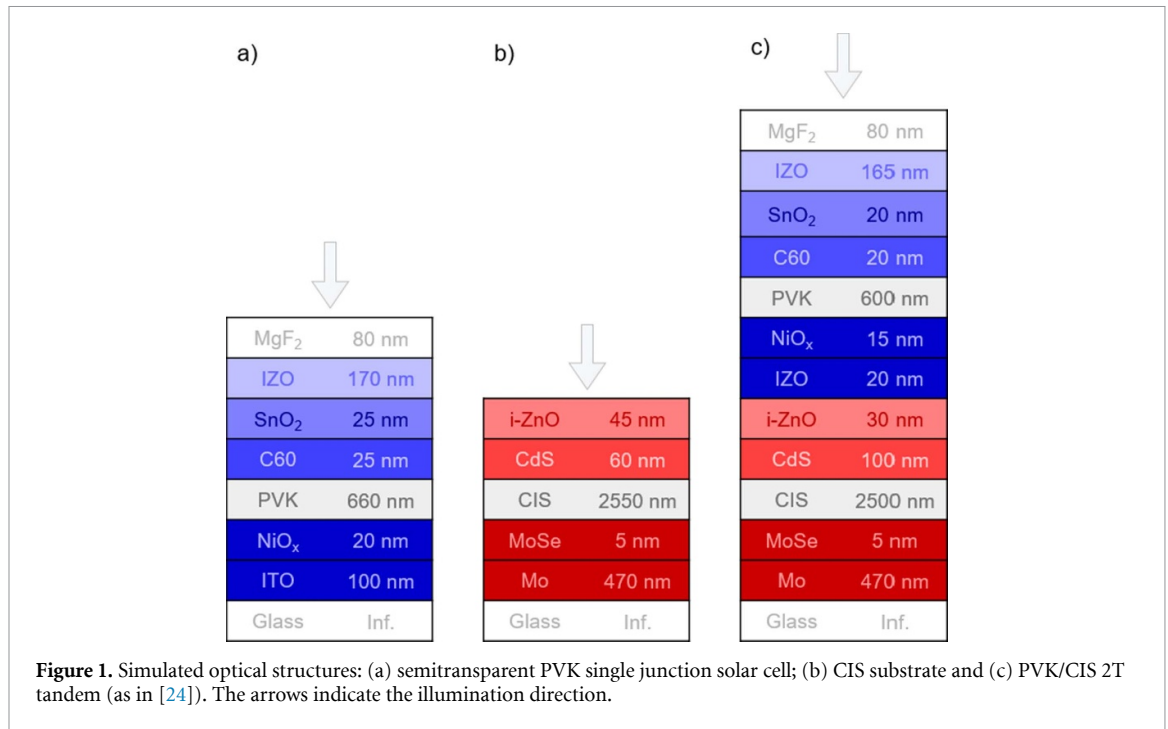### 2.1. Optical model and simulations

Optical simulations were carried out using the transfer matrix formalism [17] with a MATLAB code built in-house (further details will be published elsewhere). For this we used complex refractive indices measured experimentally by spectroscopic ellipsometry prior to this study, namely PVK ($E_g = 1.59$ eV), C_{60}, tin oxide (SnO_2), hydrogenated indium oxide (IO:H), indium tin oxide (ITO), indium zinc oxide (IZO), nickel oxide (NiO_x), and extracted from the literature, namely $CuInSe_2$ (CIS) (E_g 1.01 eV), CI(G)S (E_g 1.10 eV), molybdenum (Mo); molybdenum selenide (MoSe), aluminum-doped zinc oxide (AZO), intrinsic zinc oxide (i-ZnO), cadmium selenide (CdS) [18] and PVKs with bandgaps other than 1.59 eV [19], considered only in the last section of the results, i.e. bandgap variation. The code calculates wavelength-dependent external and internal optical properties, such as reflectance, transmittance and absorptivity of each layer. From the absorptivity in the active layer A_{abs}, we can calculate the maximal optical equivalent short-circuit current density (J_{SC}) which is an estimate of the device's real J_{SC} (assuming all photogenerated electron–hole pairs are extracted) by using (1) [20, 21]:

$$J_{SC} = q \int_0^\infty A_{abs}(\lambda) \, \Phi_{AM1.5G}(\lambda) \, d\lambda \tag{1}$$

in which q is the elementary charge and $\Phi_{AM1.5G}$ is the AM1.5G spectrum photon flux. To write equation (1) we consider that the external quantum efficiency (EQE) is equal to the absorptivity of the active layer, i.e. that the internal quantum efficiency is 100% in the active layer, and that the other layers do not contribute to current generation (the light absorbed in other layers is considered parasitic absorption). All the layers are treated as optically flat and no interface roughness is taken into account. Therefore, the light is coherent within the structure and optical interference effects will be always present in the simulations. Although models considering incoherent or partial incoherent conditions exist [22, 23] they add complexity and are not needed in the present study. Nonetheless, our approach still provides accurate results when compared to experiments, as shown later.

The optimization process was carried out step-by-step by first considering the single junction cells and then the tandem device with the simulated structures depicted in figure 1. The tandem and sub-cells have already been described in earlier publications and further information on their fabrication can be found in [24].

The structures from figure 1 only correspond to the optical part of the devices. The structure shown in figure 1(c) combines the structure of figure 1(b) which serves as the bottom sub-cell with the PVK structure

Figure 1. Simulated optical structures: (a) semitransparent PVK single junction solar cell; (b) CIS substrate and (c) PVK/CIS 2T tandem (as in [24]). The arrows indicate the illumination direction.

of figure 1(a) (with minor variations) which serves as the top sub-cell. Similar structures were fabricated and characterized to compare the results from the simulation with experimental data. The formula of the PVK used here is $Cs_{0.05}MA_{0.10}FA_{0.85}Pb(I_{0.9}Br_{0.1})_3$, with band gap of $E_g = 1.59$ eV. The 2PACz interlayer, present in the fabricated PVK device between the PVK and NiO_x, is omitted in the simulation as we have observed that it does not contribute relevantly to the optical properties due to its very small thickness of only a few molecular monolayers. The simulations were carried out in the wavelength range of 300–1300 nm, corresponding to an energy range of 0.95–4.1 eV. The direction of illumination is indicated by the arrows in figure 1, and we consider normal incidence. The thin-film structures are built on a semi-infinite glass substrate ($n = 1.5$) and are surrounded by air.

The set of refractive indices and the thicknesses of the structures shown in figure 1 were refined using an iterative process of simulation and comparison with experimental data. The importance of the exact refractive indices of the materials to use in simulations has been underlined as early as in 2014 [25], and it is still relevant. The complete list of refractive indices used in this work can be found in the SI.

2.2. Experimental methods

The simulated data is relevant only if it can be supported by the experimental results of the same device structures. For this, we measured the samples of the structures shown on the figure 1 by two complementary techniques: EQE and reflectance (R), described in SI. The structure from the figure 1(b) is not a working solar cell, since it lacks a transparent conductive oxide (TCO) top electrode, for which it has been characterized only using reflectance measurements.

3. Results

3.1. Model validation by comparison to experimental results

First, we simulated the structures presented in figure 1 and compared the resulting EQE and reflectance to the experimental results, to verify the model (i.e. the selection of refractive indices and thicknesses). Within an iterative process we found the thicknesses and refractive indices of the layers, so that the simulated results match well the experimental data (see figure 2). The complete list of the complex refractive indices used in this work can be found in the SI.

We show the final results of the simulated models compared with experimental EQE and R in figure 2. In figure 2(a) we observe a good match for the EQE of the PSC, where the shape follows well the experimental points. However, the reflectance spectra are deviating from the experimental one at near-infrared (NIR) wavelengths. This is caused here by the strong reflection from the inadvertently illuminated silver contacts, that were present in the real sample which significantly increased measured reflectance. Nevertheless, the spectral region from 300 to 800 nm is well reproduced by the simulated curve. In case of the CI(G)S bottom
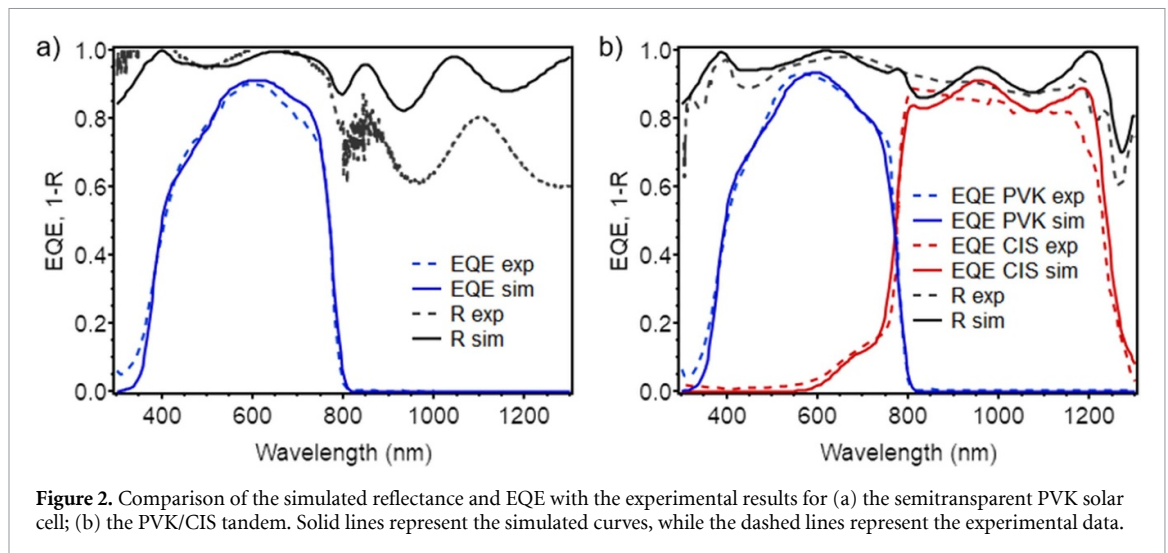
Figure 2. Comparison of the simulated reflectance and EQE with the experimental results for (a) the semitransparent PVK solar cell; (b) the PVK/CIS tandem. Solid lines represent the simulated curves, while the dashed lines represent the experimental data.

sub-cell, the results of simulations are much closer to the experimental ones. We can see in figure S1(a) that the simulated reflectance matches the experiment, with only small deviations in the NIR region. As a reminder, the code used for simulations does not consider incoherent effects nor the roughness, which can cause the reflectance minima and maxima to be much more pronounced in the simulated curves, while in the experimental data the amplitude of these features is less distinct [18]. As long as the wavelength positions of minima and maxima of the interference fringes in the reflectance spectrum matches to those in the experimental spectrum, together with a good match of the average values of *R* and EQE, we consider the result sufficient. We note that since the CI(G)S bottom sub-cell does not contain the top TCO layer, the EQE has been not measured. Verification was based only on the reflectance spectrum.

After the individual assessment of the PVK semitransparent solar cell and CIS substrate, the two models were combined to simulate the tandem device. For the single solar cell, we used commercial substrate of ITO-covered glass slides, whereas in case of the tandem architecture, the recombination layer was IZO. For this reason, in the model we also substituted the TCO material, i.e. the ITO of the semitransparent PSC (figure 1(a)) with an IZO film (figure 1(c)) and adjusted the thicknesses of the other layers. The optimization process consisted of simulating the *R* and EQE spectra for different thicknesses of one layer at a time, and selecting the result that best fitted the experimental data. The thicknesses were kept always in the range of experimentally acceptable values. That is, the thicknesses were in accordance to the production method limitations as for instance it would not be possible to produce very thin layers of some materials, because resulting thin films do not provide homogeneous coverage, or simply to assure good enough electrical properties as is the case especially for TCOs. Since in this work we were not simulating the electrical properties, these thicknesses were selected based on our calibrated nominal TCO layer thickness. The optical response of the optimized tandem model is depicted in figure 2(b), showing a good match between model and experiment for the wavelength range from 300 to 800 nm. In the NIR region (800–1300 nm), the fit is perturbed by interference effects in the *R* and EQE spectra. This is caused by the fact, that the real samples have some roughness which is not considered in the simulation, and this leads to some partial incoherence and deviation between experiments and simulations, especially for longer wavelengths.

We then calculated J_{sc} by integrating the experimental and simulated EQE spectra, to further constrain the model, by comparing the values of the current density generated in the absorbers. In the experimental PSC, the generated J_{sc} from EQE spectra equals 19.4 mA cm^{-2}, while from the simulated model we find a J_{sc} of 20.2 mA cm^{-2}. For the CI(G)S bottom sub-cell, the J_{sc} generated in the absorber was 39.6 mA cm^{-2}, which is in range of J_{sc} values obtained for CIS cells [26]. However, we note that in the presence of the top TCO electrode this value would probably be lower due to increased parasitic absorption in the UV-range (300–400 nm), and possible free carrier absorption in the NIR. For the tandem solar cell, the current density generated in the PVK sub-cell is 20.3 mA cm^{-2}, both in the experimental and simulated data with an excellent match to the integrated EQE of this sub-cell. The current density generated in the CIS sub-cell was 21.2 mA cm^{-2} determined experimentally and 21.3 mA cm^{-2} derived from the simulation, proving that average values of the interference-impacted regions are resulting in a J_{sc} comparable to the measured one. This also indicates that the current limiting sub-cell in the tandem is the PSC, for which we can attribute a loss of 1 mA cm^{-2}, due to the current mismatch between the sub-cells. The precise values of the current density calculations can be found in the SI (table S1 and figure S2).
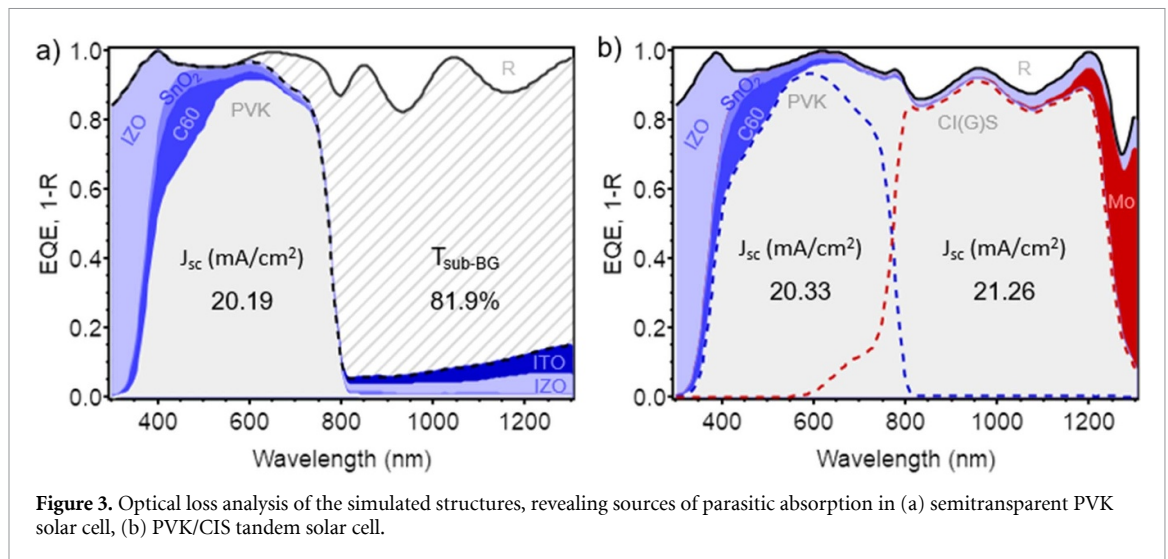
Figure 3. Optical loss analysis of the simulated structures, revealing sources of parasitic absorption in (a) semitransparent PVK solar cell, (b) PVK/CIS tandem solar cell.

3.2. Optical loss analysis

In the following we use the models described above as a starting point for the optimization of the tandem structure to reach higher efficiencies beyond the reported record of 24.9% [24]. In this regard, a detailed optical loss analysis of the simulated structures, as shown in figure 3, allows us to identify layers which are the sources of strong parasitic absorption—that is, the light that has been absorbed by this layer does not contribute to the J_{sc} of the device.

In case of the semitransparent PSC (figure 3(a)), the largest loss is due to the thick top TCO layer (170 nm of IZO), which absorbs almost 10% of the incident illumination (see table S2 in the SI). Also, C_{60} is a significant source of parasitic absorption. In the NIR part of the graph (780–1300 nm) we observe significant free carrier absorption in the sub-bandgap region in both TCOs, resulting in a decrease in transmittance of the PSC top cell. TCOs and C_{60} have been already identified as a main parasitic absorption sources in PVK-based solar cells [15, 27–30], underlining the need to optimize these layers.

Analyzing the optical losses of the CIS sub-cell (figure S1(b) and table S2), we observe very strong parasitic absorption in i-ZnO and CdS layers. For tandems, however, this does not account for a major loss, because photons in the wavelength range absorbed in these layers (300–600 nm) will be already fully absorbed by the PVK film in the top sub-cell. Their thicknesses, however, can play a role in the total reflectance spectrum of the tandem device, thus, we also considered them in the optimization of the tandem device. In this work, the rest of the CIS sub-cell will not be optimized, however we refer the interested reader to further publications related to this task [18, 31, 32].

Last, the optical loss analysis of the tandem shown in figure 3(b) suggests that the part for which we can reach the largest improvement is the PVK top sub-cell, as it is the one where the highest share of parasitic absorption occurs. Similarly, to the semitransparent solar cell (figure 3(a)), the IZO top electrode is responsible for the main losses in the UV–VIS range.

These analyses allowed us to formulate clear goals for the optimization procedure. First, the semitransparent PSC (figure 1(a)) needs to be optimized, to (i) increase sub-bandgap transmittance and (ii) maximize the generated current density by decreasing parasitic absorption in the functional layers and minimizing the reflectance. The threshold value of the sub-bandgap transmittance (T_{sub-BG}—below the band gap of PVK $E_g = 1.59$ eV, corresponding to a wavelength of 780 nm) is more than 90%. T_{sub-BG} is defined as the ratio of the integrated area below the transmittance curve in the range 780–1300 nm to the sum of the $A + R + T$ in the same wavelength range. Similarly, any percentage values of R, A or T given later are defined in the same way, but in the full range of wavelengths (300–1300 nm). Finally, the optimized PVK sub-cell will be integrated into the tandem model as a starting point with subsequent adjustments of all layers, in order to maximize the current generated in both absorbers (PVK and CIS) and achieve current matching between the two sub-cells.

3.3. Optimization of the devices

In the semitransparent PVK solar cell optimization, we first optimized the top TCO thickness (170 nm IZO), which has been identified as the main source of parasitic absorption in the UV-region. Several TCO materials are considered as suited for top electrodes in PVK-based solar cells, including IZO, ITO, and IO:H [8–10, 15, 29]. We have simulated the J_{sc} and sub-bandgap transmittance of the PVK solar cell with IZO and IO:H of

various thicknesses as the top TCO layer, shown in the supplementary information in figure S3(a). Devices with ITO for the top electrode have also been simulated in this work, however, this material exhibits inferior optical properties compared to IZO and IO:H, and hence we have excluded it from further consideration. In figure S3(a) we can see a result of this optimization. By enabling more light to reach the PVK absorber, the solar cell with IO:H as the top TCO achieves higher current densities than the solar cell employing IZO. Also, sub-bandgap transmittance is higher in this case. In figure S3(a) we observe that for both TCOs the J_{sc} values exhibit minima for the thickness values between 50 and 120 nm.

Since there was no particular current density established as a goal of this optimization, the $T_{sub-BG} > 90\%$ was first considered when selecting the appropriate TCO thickness. Any of the thicknesses of both materials allows to reach 90% transmittance; moreover, the maximum transmittance corresponded to the thicknesses with the lowest achievable J_{sc} of the device. From an optical point of view, a thinner TCO will result in better transmittance, however if the TCO layer is too thin it will not provide sufficient electrical conductivity. For this reason, we decided to select IO:H of the thickness of 130 nm as the top contact, which will provide high NIR transmittance of the PVK top sub-cell, while being thick enough to exhibit good electrical conductivity.

We applied a similar procedure for the optimization of the rear TCO in the PSC device. Here, to exchange the ITO, which was resulting in very high NIR parasitic absorption due to free carrier absorption, we considered two other materials: IZO and AZO. All these materials are often used in state-of-the-art PVK/CI(G)S tandem devices [14, 24, 33–35]. In this optimization step, we observe almost no change to the current density, which is as expected, since this TCO layer is located below the PVK absorber. The main goal was to further increase the sub-BG transmittance. In figure S3(b) we can see that AZO layer is resulting in much better transmittance than rear IZO (both layers result in similar current densities of the device). For AZO thicknesses of 70–120 nm, the transmittance is between 89% and 90%. While it can appear counterintuitive at first glance, that the transmittances increase with increasing TCO thickness, the improvement is explained by the decrease in the reflectance spectrum. Since $A + T + R = 1$ (or 100%), we attribute the decrease of reflectance as the source for improved transmittance, even if the absorption in the TCO is increased due to its increased thickness. This relation is shown in figure S4. We can conclude, that AZO as the rear TCO can act as antireflective coating, as its refractive index is in-between that of NiO_x and glass, and hence increase the photo-generated current with increasing thickness.

Thus, the AZO layer with a thickness of 110 nm has been selected as a replacement of the 100 nm thick ITO layer. Although, the optimum may further change later in case of the tandem stack, since here we consider the AZO/glass interface and will need to include the full CIS sub-cell in between them, which results in best improvement of the optical performance for the semitransparent solar cell. Some other minor changes allowed us to eventual reach a J_{sc} of 21.8 mA cm^{-2} generated in the PVK absorber, while a sub-bandgap transmittance of 92% is maintained. These adjustments include decreasing the thickness of C_{60} and SnO_2 from 20 to 12 nm. The lower the thickness of these layers, the lower the parasitic absorption. However, layers thinner than 10 nm can be challenging to deposit and exhibit inferior electrical properties. Hence we did not decrease their thickness any further. Furthermore, the thickness of the antireflection coating (MgF_2) has been increased from 80 to 100 nm. The final spectra with the concomitant optical loss analysis and the final structure are shown in figure 4. Detailed absorption analysis is listed in the table S2.

The new PVK sub-cell from figure 4 has been directly applied to the tandem stack, which already enabled us to decrease the parasitic absorption in the UV and blue spectral region with a concomitant increase of absorption in the PVK absorber. However, the following additional adjustments were necessary for the tandem configuration, to obtain higher current density in both sub-cells and the corresponding current matching. We decreased the AZO thickness to 80 nm and changed the thickness of the i-ZnO and CdS layers, which do not absorb any significant amount of light in the tandem configuration (see table S2 in the SI), to obtain a more favorable reflectance. As has been already noted by Jost *et al* [14], it is possible to find many thickness pairs of these two materials that allow to increase the absorption in the CIS sub-cell. Here, for the tandem configuration, the optimal results were obtained for an increase of the i-ZnO thickness from 30 nm to 50 nm, and a decrease in the CdS thickness from 100 nm to 80 nm. Finally, we adjusted the PVK layer thickness to an optimal value of 640 nm (figure S5), which had the highest impact on the current matching.

With such optimized tandem, we obtained almost ideally matched J_{sc} of more than 21.7 mA cm^{-2} (21.75 in PVK sub-cell and 21.76 in CIS sub-cell). This improves the initial J_{sc} of the tandem device by almost 1.5 mA cm^{-2}. The final structure and the corresponding R and EQE spectra with optical loss analysis are shown in figure 5.

The results of the optical loss analysis of the initial structures from figure 1 ('start') and final optimized structures from figures 4 and 5 ('optimized') are presented in figure 6. The comparison shows the distribution of the optical properties in the devices (that is, the fraction of incident light that is absorbed in, reflected from, and transmitted through the device), distinguishing the absorption in the active layer (absorbers: PVK and CIS) in light green, parasitic absorption A_{par} in dark green, reflectance R in blue, and
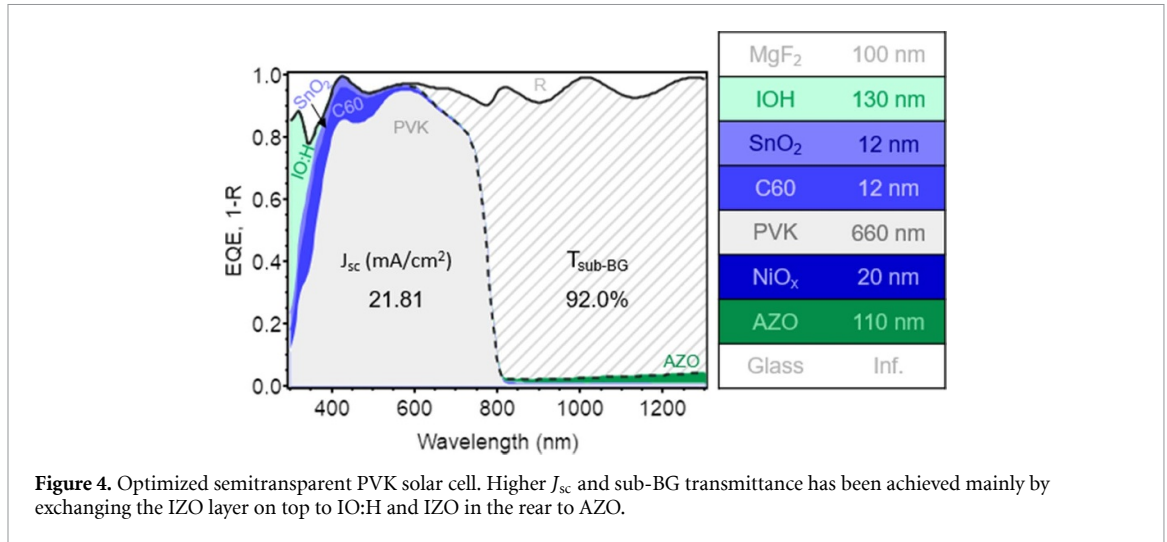
Figure 4. Optimized semitransparent PVK solar cell. Higher J_{sc} and sub-BG transmittance has been achieved mainly by exchanging the IZO layer on top to IO:H and IZO in the rear to AZO.
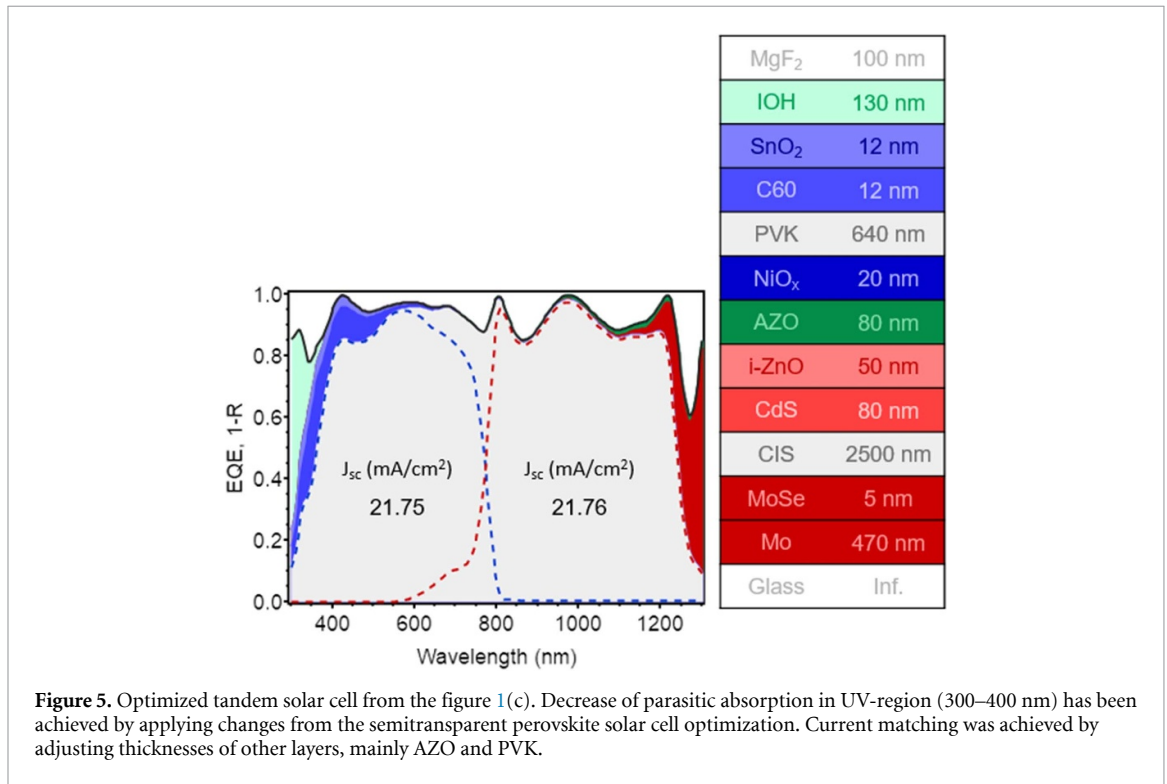

Figure 5. Optimized tandem solar cell from the figure 1(c). Decrease of parasitic absorption in UV-region (300–400 nm) has been achieved by applying changes from the semitransparent perovskite solar cell optimization. Current matching was achieved by adjusting thicknesses of other layers, mainly AZO and PVK.
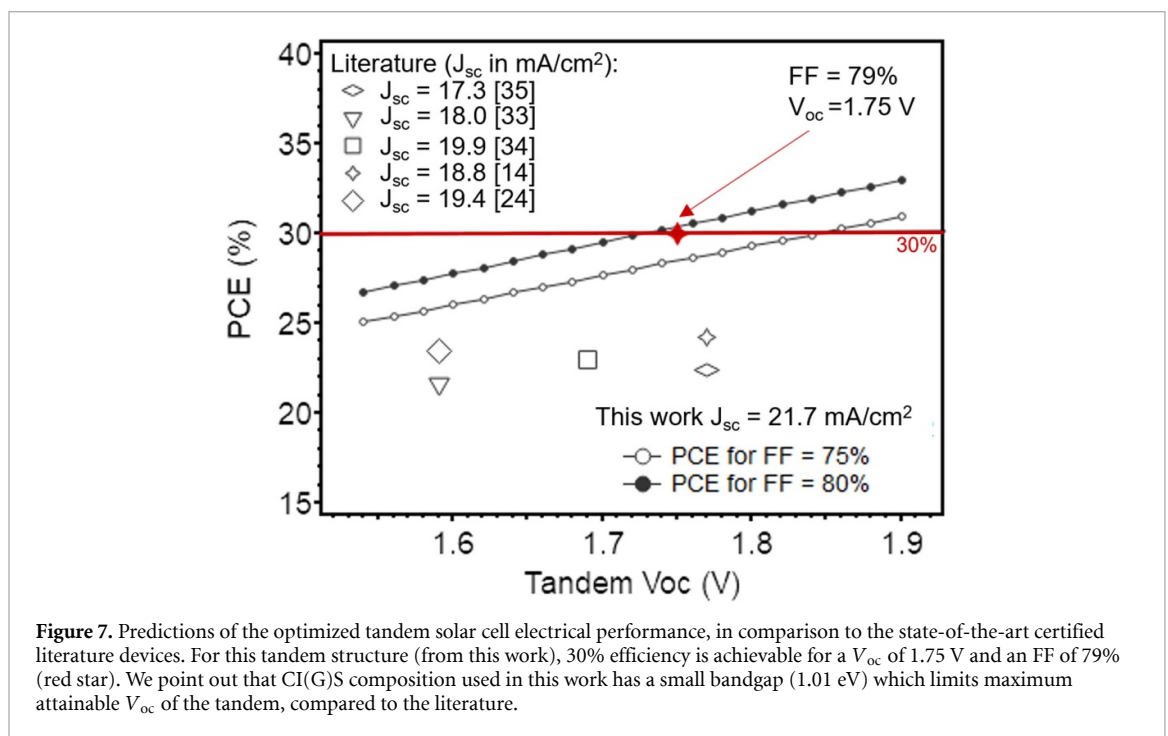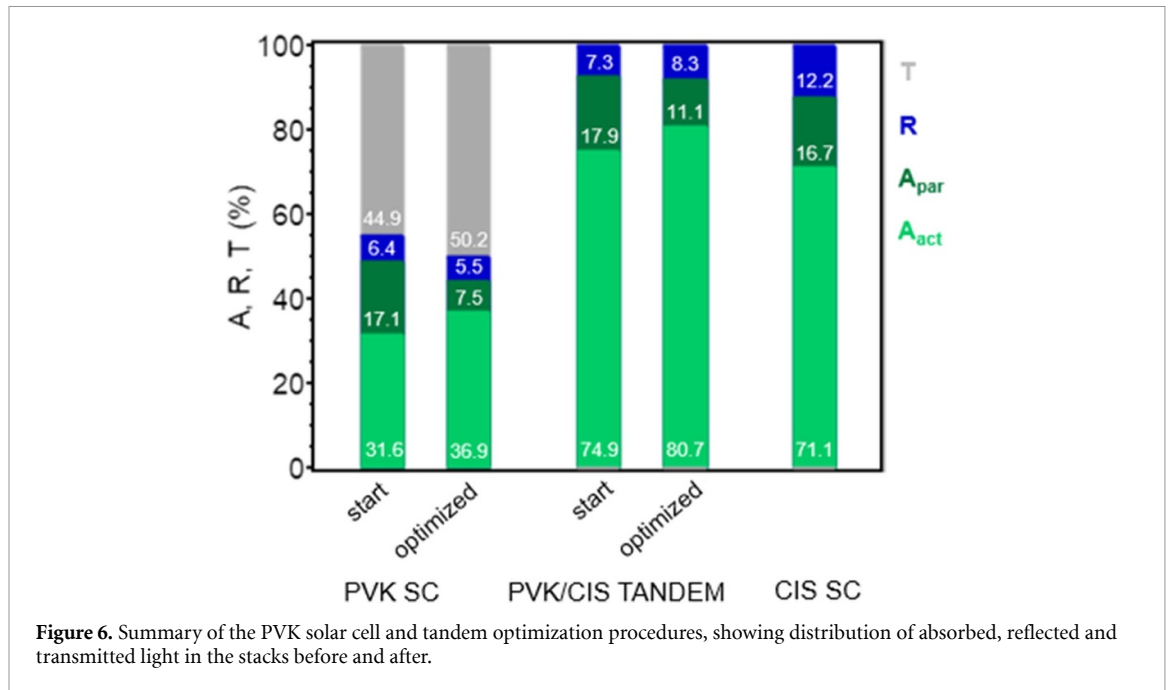
transmittance T in grey. All distributions fulfill the condition: $1 = (A_{act} + A_{par}) + R + T$ and clearly indicate that the key to increasing the absorption in the active layers to finally increase J_{sc} is to decrease the parasitic absorption by selecting more adequate materials with adjusted thickness values.

3.4. Tandem cell performance

Going beyond optical simulations, we use the results of the optical optimization to predict achievable efficiencies of such cells (figure 7). Sha *et al* for example, calculated the efficiency limit of PVK single solar cells of about 31% (using detailed balance model) [36]. For tandems, Chen *et al*, predicted 29% efficiency for PVK/CI(G)S tandems [37] if the tandem has an optimized design. Since our work is strictly focused on optical simulations, the values for open circuit voltage V_{oc} and fill factor (FF) that are required for the calculation of the PCE have been selected by revising the results for the state-of-the-art PVK/CI(G)S tandem devices.

First, as a general observation we find that the best-performing PVK/CI(G)S tandems have very similar device configuration [14, 24, 33, 35]: IZO as a top electrode, SnO_2/C_{60} (or PCBM) as an electron transport layer, ETL, NiO_x with self-assembled monolayers (SAMs), or SAMs alone, as a hole transport layer, HTL. The most-used TCO for the recombination layer is AZO, while the CI(G)S bottom-cell configuration remains

Figure 6. Summary of the PVK solar cell and tandem optimization procedures, showing distribution of absorbed, reflected and transmitted light in the stacks before and after.

Figure 7. Predictions of the optimized tandem solar cell electrical performance, in comparison to the state-of-the-art certified literature devices. For this tandem structure (from this work), 30% efficiency is achievable for a V_{oc} of 1.75 V and an FF of 79% (red star). We point out that CI(G)S composition used in this work has a small bandgap (1.01 eV) which limits maximum attainable V_{oc} of the tandem, compared to the literature.

almost the same. The optimized structure in this work is also very similar to those, with the main difference being the top TCO IO:H instead of IZO. We can thus assume that such structure would reach similar values of the FF and V_{oc}. For the V_{oc}, there is a spread of different values that are reached by tandem cells in literature ranging from 1.59 V to 1.77 V (current record devices [14, 24]). Since this parameter depends strongly on the bandgaps of the absorbers, film quality and non-radiative recombination, we decided to calculate the PCE using V_{oc} for the broad range of values from 1.5 V to 1.9 V. Considering best performing small bandgap CIS ($E_g = 1.01$ eV) and PVK (1.59 eV) single solar cells, these devices can reach V_{oc} on the order of 0.6 V [38, 39] and 1.1 V respectively. Regarding the FF, we selected two values to also provide a range of possible combinations of V_{oc} and FF. An FF = 75% is currently achieved in the state-of the-art devices, and FF = 80% is assumed to be achievable in practice [14]. With this, we can see that the optimized tandem device of this work would be able to reach PCE > 30% for the $V_{oc} = 1.75$ V, and FF of 79%. These values
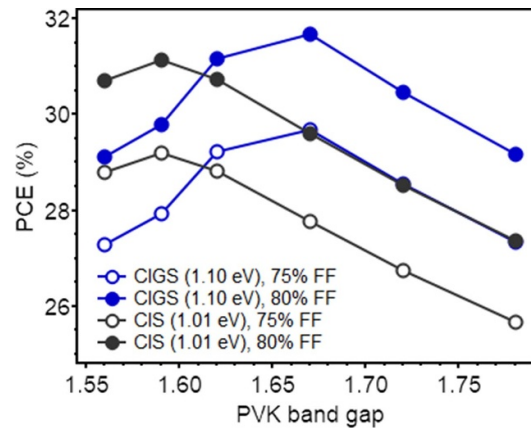
Figure 8. Power conversion efficiency (PCE) predictions for the structure from the paper with different perovskite bandgaps and with two different bottom cell bandgaps; CI(G)S ($E_g = 1.10$ eV) in blue and CIS ($E_g = 1.01$ eV) in black.

might be quite challenging to achieve for such bandgap selection for the absorbers (1.01 eV for CI(G)S and 1.59 eV for PVK), especially assuming quite high idealized current from these simulations of 21.7 mA cm^{-2} and high FF of almost 80%. Nevertheless, with this new optimized stack (figure 5), 30% efficiency of CIS/PVK 2T tandem should be within our reach. These improvements could include: passivation to increase V_{oc} by decreasing non-radiative recombination or trying different bandgap combination of the absorbers. To increase fill factor, management of parasitic resistances (shunt and sheet resistances) would need to be achieved by improving solar cell manufacturing processes.

Our work thus gives the following perspectives for the current PVK/CI(G)S tandem development direction:

- Exchanging top TCO to IO:H would allow to reach J_{sc} higher than 21 mA cm^{-2} (current highest certified J_{sc} from mentioned tandem structures from the literature is 19.9 mA cm^{-2} [34]).
- With no more significant material changes in this tandem stack, the >30% efficiencies will by possible by slightly improving V_{oc} to 1.75 V and FF to 79%.

This would allow PVK/CI(G)S tandems to catch up with PVK/c-Si technology.

3.5. Bandgap variation

Furthermore, we simulated the J_{sc} of the tandem structure from figure 5 using PVKs with different bandgaps (1.56 eV, 1.62 eV, 1.67 eV, 1.72 eV and 1.78 eV) and also bottom sub-cell absorbers with two different bandgaps: CI(G)S with bandgap 1.10 eV, typically used in PVK/CI(G)S tandems in literature, and small bandgap CI(G)S, here referred as CIS of a bandgap 1.01 eV used for our cells. Different bandgaps will not only change the theoretically attainable V_{oc} of the tandem, but will also change the amount of absorbed light by each sub-cell and thus generated J_{sc}. Refractive indices of the PVK absorbers of different band gaps mentioned in this section has been found in the literature [19].

In our simulations using the optimized structure from figure 5, we simulated J_{sc} for the different bandgaps of the absorbers. The thickness of the PVK absorber was systematically varied to ensure current matching. When it was possible—we then selected this thickness and the corresponding J_{sc} of the tandem. However, achieving current matching conditions for most of the bandgap combinations in this structure was impossible. In such cases, the current of the limiting sub-cell has been selected as the tandem J_{sc}, for the PVK thickness that resulted in the 'closest' current matching conditions possible.

Having simulated J_{sc} of the tandem devices with different absorber bandgaps, we then estimated attainable V_{oc} based on the bandgaps. Following Jost *et al* [14], we assumed a V_{oc} loss of 400 mV for the PVK, and for CI(G)S cases, we assumed the max V_{oc} currently achievable in stand-alone solar cells. For CIS (1.01 eV) it was 600 mV and for CI(G)S (1.10 eV) it was 730 mV. Again, for the predictions we used two fill factors: 75% being the currently achievable in the literature for 2T PVK/CI(G)S tandems and a theoretically achievable FF = 80% for the reference.

The results are shown in figure 8. We can see that for larger bandgap absorbers (both PVK and CI(G)S), the attainable *PCE* is higher compared to the cases with smaller bandgaps. The maximum corresponds to the PVK (1.67 eV)/CI(G)S (1.10 eV) combination, achieving almost 32% efficiency for FF = 80%. For small bandgap CIS, the best bandgap of PVK appears to be the one used in our work (1.59 eV), leading to 30% efficiency as discussed before (figure 7).

4. Conclusion

We present a dedicated framework of optical simulations to predict the performance of monolithic CI(G)S/PVK tandem solar cells that allow for a successive optimization of the device stack to reduce optical losses and achieve current matching of the two sub-cells. Our transfer matrix calculations require only material thickness and the complex refractive indices of the materials as input and hence enable an efficient simulation procedure which we verify with corresponding experimental data. We attribute the principal optical losses to the TCO films and thus exchanging IZO by AZO in the recombination layer between the individual sub-cells reduced the parasitic absorption. Improved current matching was achieved by changing the thickness of the various layers in the device stack and notably by increasing the thickness of the PVK absorber. From our optical simulations and the calculated J_{sc} values, we then derive, considering realistic solar cell parameters, that an efficiency of over 30% can be obtained in this optimized geometry. Notably, we find by changing the bandgap of the absorber layers, that a CI(G)S band gap of 1.1 eV with a PVK band gap of 1.67 eV yield maximum performance values. While this relaxes the technological requirements for the CI(G)S sub-cell, further work on the large-band gap PSC would be required to reach optimal values. However, successful integration of low band gap CI(G)S sub-cells (1.01 eV) would enable the use of PVK layers with 1.6 eV band gap without major detriment to the device performance. At these examples, our work hence demonstrates how the development of the next generation of monolithic CI(G)S/PVK tandem devices can be accelerated by the dedicated iterative optimization procedure of the optical properties of each layer in the stack.

Data availability statement

All data that support the findings of this study are included within the article (and any supplementary files).

Acknowledgments

Author contributions

Original draft A B, P S; draft review and editing: all the authors; optical simulations A B with support from D M; OptiPV TMM code provided by D M, M G, S C and J-F G; EQE measurements A B with support from K M; photospectrometry A B; semitransparent perovskite solar cells and tandem solar cells provided by M A R-P and U W P; CIS solar cells and bottom sub-cells provided by V S G and M S; complex refractive indices of CI(G)S solar cells provided by R C; CI(G)S expertise shared by: N N, R C, V S G and M S; supervision: P S, J-F G, S C, U W P.

Conflict of interest

Authors declare no conflict of interest.

ORCID iDs

Aleksandra Bojar ⬥ https://orcid.org/0000-0001-9712-7646
Stéphane Collin ⬥ https://orcid.org/0000-0001-6176-1653

References

[1] Green M, Dunlop E D, Siefer G, Yoshita M, Kopidakis N, Bothe K and Hao X 2023 Solar cell efficiency tables (Version 61) *Prog. Photovolt. Res. Appl.* **31** 3–16

[2] Micha D N and Silvares Junior R T 2019 The influence of solar spectrum and concentration factor on the material choice and the efficiency of multijunction solar cells *Sci. Rep.* **9** 20055

[3] Micha D N and Silvares Junior R T 2021 A self-consistent interactive model for the study of luminescence coupling in multijunction solar cells *J. Appl. Phys.* **130** 243103

[4] Saliba M, Correa-Baena J-P, Grätzel M, Hagfeldt A and Abate A 2018 Perovskite solar cells: from the atomic level to film quality and device performance *Angew. Chem., Int. Ed.* **57** 2554–69

[5] Guiliano G, Bonasera A, Arrabito G and Pignataro B 2021 Semitransparent perovskite solar cells for building integration and tandem photovoltaics: design strategies and challenges *Phys. Status Solidi* **5** 2100702

[6] De Wolf S, Holovsky J, Moon S-J, Löper P, Niesen B, Ledinsky M, Haug F-J, Yum J-H and Ballif C 2014 Organometallic halide perovskites: sharp optical absorption edge and its relation to photovoltaic performance *J. Phys. Chem. Lett.* **5** 1035–9

[7] Wang Z, Song Z, Yan Y, Liu S and Yang D 2019 Perovskite—a perfect top cell for tandem devices to break the S-Q limit *Adv. Sci.* **6** 1801704

[8] Stranks S and Snaith H J 2015 Metal-halide perovskites for photovoltaic and light-emitting devices *Nat. Nanotechnol* **10** 391–402

[9] Biao S *et al* 2019 Semitransparent perovskite solar cells: from materials and devices to applications *Adv. Mater.* **32** 1806474

[10] Correa-Baena J P, Abate A, Saliba M, Tress W, Jesper Jacobsson T, Grätzel M and Hagfeldt A 2017 The rapid evolution of highly efficient perovskite solar cells *Energy Environ. Sci.* **10** 710–27

[11] Sobayel K, Shahinuzzaman M, Amin N, Karim M R, Dar M A, Gul R, Alghoul M A, Sopian K, Hasan A K M and Akhtaruzzaman M 2020 Efficiency enhancement of CIGS solar cell by WS$_2$ as window layer through numerical modelling tool *Sol. Energy* **207** 479–85

[12] Carron R *et al* 2019 Advanced alkali treatments for high-efficiency Cu(In,Ga)Se$_2$ solar cells on flexible substrates *Adv. Energy Mater.* **9** 190040

[13] Green M A and Ho-Baillie A W 2019 *ACS Energy Lett.* **4** 1639–44

[14] Jost M *et al* 2022 Perovskite/CIGS tandem solar cells: from certified 24.2% toward 30% and beyond *ACS Energy Lett.* **7** 1298–307

[15] Jost M, Kegelmann L, Korte L and Albrecht S 2020 Monolithic perovskite tandem solar cells: a review of the present status and advanced characterization methods toward 30% efficiency *Adv. Energy Mater.* **10** 104102

[16] Kurtz S R, Faine P and Olson J M 1990 Modeling of two-junction, series-connected tandem solar cells using top-cell thickness as an adjustable parameter *J. Appl. Phys.* **68** 1890

[17] Centurioni E 2005 Generalized matrix method for calculation of internal light energy flux in mixed coherent and incoherent multilayers *Appl. Opt.* **44** 7532–9

[18] Carron R *et al* 2018 Refractive indices of layers and optical simulations of Cu(In,Ga)Se$_2$ solar cells *Sci. Technol. Adv. Mater.* **19** 396–410

[19] Ndione P, Li Z and Zhu K 2016 Effects of alloying on the optical properties of organic–inorganic lead halide perovskite thin films *J. Mater. Chem.* C **4** 7775–82

[20] Massiot I, Cattoni A and Collin S 2020 Progress and prospects for ultrathin solar cells *Nat. Energy* **5** 959–72

[21] Nelson J 2003 *The Physics of Solar Cells* 1st edn (London: Imperial College Press) (https://doi.org/10.1142/p276)

[22] Raoult E, Bodeux R, Jutteau S, Rives S, Yaiche A, Blaizot A, Coutancier D, Rousset J and Collin S 2022 Iterative method for optical modelling of perovskite-based tandem solar cells *Opt. Express* **30** 9604–22

[23] Raoult E *et al*, 2019 Optical characterisations and modelling of semitransparent perovskite solar cells for tandem applications *36th European Photovoltaic Solar Energy Conf. and Exhibition* (https://doi.org/10.4229/EUPVSEC20192019-3BV.2.53)

[24] Ruiz-Preciado M *et al* 2022 Monolithic two terminal perovskite/CIS tandem solar cells with efficiency approaching 25% *ACS Energy Lett.* **7** 2273–81

[25] Ziang X *et al* 2015 Refractive index and extinction coefficient of CH$_3$NH$_3$PbI$_3$ studied by spectroscopic ellipsometry *Opt. Mater. Express* **5** 29–43

[26] Nakamura M, Yamaguchi K, Kimoto Y, Yasaki Y, Kato T and Sugimoto H 2019 Cd-free Cu(In,Ga)(Se,S)$_2$ thin-film solar cell with record efficiency of 23.35% *IEEE J. Photovolt.* **9** 1863–7

[27] Manzoor S, Häusele J, Bush K A, Palmstrom A F, Carpenter J, Yu Z J, Bent S F, Mcgehee M D and Holman Z C 2018 Optical modelling of wide-bandgap perovskite and perovskite/silicon tandem solar cells using complex refractive indices for arbitrary bandgap perovskite absorbers *Opt. Express* **26** 27441–60

[28] van Eerden M, Jaysankar M, Hadipour A, Merckx T, Schermer J J, Aernouts T, Poortmans J and Paetzold U W 2017 Optical analysis of planar multicrystalline perovskite solar cells *Adv. Opt. Mater.* **5** 1700151

[29] Ball J M *et al* 2015 Optical properties and limiting photocurrent of thin-film perovskite solar cells *Energy Environ. Sci.* **8** 602

[30] Pisoni S, Carron R, Moser T, Feurer T, Fu F, Nishiwaki S, Tiwari A N and Buecheler S 2018 Tailored lead iodide growth for efficient flexible perovskite solar cells and thin film tandem devices *NPG Asia Mater.* **10** 1076–85

[31] Bernal-Correa R, Morales-Acevedo A, Montes-Monsalve J and Pulzara-Mora A 2016 Design of the TCO (ZnO:Al) thickness for glass/TCO/CdS/CIGS/Mo solar cells *J. Phys. D: Appl. Phys.* **49** 125601

[32] Dabbabi S, Nasr T B and Kamoun-Turki N 2017 Parameters optimization of CIGS solar cells using 2D physical modelling *Results Phys.* **7** 4020–4

[33] Jost M *et al* 2019 21.6% efficient monolithic perovskite/Cu(In,Ga)Se$_2$ tandem solar cells with thin conformal hole transport layers for integration on rough bottom cell surfaces *ACS Energy Lett.* **4** 583–90

[34] Al-Ashouri A *et al* 2019 Conformal monolayer contacts with lossless interfaces for perovskite single junction and monolithic tandem solar cells *Energy Environ. Sci.* **12** 3356

[35] Han Q *et al* 2018 High-performance perovskite/Cu(In, Ga)Se$_2$ monolithic tandem solar cells *Science* **361** 904–8

[36] Sha W E I, Ren X, Chen L and Choy W C H 2015 The efficiency limit of CH$_3$NH$_3$PbI$_3$ perovskite solar cells *Appl. Phys. Lett.* **106** 221104

[37] Chen C-W, Hsiao S-Y, Chen C-Y, Kang H-W, Huang Z-Y and Lin H-W 2015 Optical properties of organometal halide perovskite thin films and general device structure design rules for perovskite single and tandem solar cells *J. Mater. Chem.* A **3** 9152–9

[38] Feurer T, Carron R, Torres Sevilla G, Fu F, Pisoni S, Romanyuk Y E, Buecheler S and Tiwari A N 2019 Efficiency improvement of near-stoichiometric CuInSe$_2$ solar cells for application in tandem devices *Adv. Energy Mater.* **9** 1901428

[39] Feurer T, Fu F, Weiss T P, Avancini E, Löckinger J, Buecheler S and Tiwari A N 2019 RbF post deposition treatment for narrow bandgap Cu(In,Ga)Se$_2$ solar cells *Thin Solid Films* **670** 34–40